ORIGINAL ARTICLE

# Antidiabetic and oxidative stress assessment of bio-enzymatically synthesized zinc oxide nanoformulation on streptozotocin-induced hyperglycemic mice

Faizan Ahmed[1] · Qayyum Husain[1] · Mohd Owais Ansari[2] · G. G. H. A. Shadab[2]

## Abstract

Oxidative stress has significant contribution in on-set and progression of diabetes. The disease onset leads to elevated levels of free radicals rendering the oxidant-inducing mechanisms incapable of protecting cellular organelles from inflicted damage. Herein, β-galactosidase-mediated bio-enzymatic synthesis of zinc oxide nanoparticles (ZnO NPs) was pioneered and characterized. These obtained ZnO NPs were assessed for their antidiabetic activity against streptozotocin (STZ)-induced diabetic mice. For this objective, 36 male albino mice were separated into 6 groups. The diabetes was induced in mice with STZ (120 mg $kg^{-1}$ body weight), and further treated with three different doses of ZnO NPs (0.5 mg $kg^{-1}$, 1 mg $kg^{-1}$, and 2 mg $kg^{-1}$) for 28 days. The results unveiled protective effects in diabetic mice treated with ZnO NPs through restoration of changes in body weight and normal glucose levels. The effects of ZnO NPs on lipid peroxidation and carbonyl contents were protective in liver, kidney and pancreas of diseased groups. Levels of serum biomarkers such as cholesterol, triglycerides and HDL-C indicated ZnO NPs treatment caused these levels to plummet towards control parameters. Normal liver function markers and urea levels in serum indicated successful treatment of diabetic mice with ZnO NPs. Histopathological studies revealed protective and non-toxic effects of ZnO NPs over vital tissues of kidney, liver, and pancreas. The results divulge efficacious pharmaceutical potential of ZnO NPs against formation of reactive oxygen species by scavenging free radicals enhancing the functioning of antioxidant fortifying enzymes generating sustenance over hyperglycemic conditions.

**Keywords** Zinc oxide nanoparticles · β-Galactosidase · Hyperglycemia · Oxidative stress · Antidiabetic · Nanodrug

## Introduction

Untreated hyperglycemic condition causes widespread dis-functioning of organs in human body within due course of time. Amongst the two major forms of diabetes, type 2 diabetes has broader influence over population all around the world (Tahrani et al. 2011). The condition arises through onset of chronic metabolic disorder, diabetes mellitus, due to deficient insulin production by pancreatic β cells, owing to adverse genetic, metabolic and environmental factors (He et al. 2017). Unrestricted hyperglycemia might lead to numerous complications including cardiovascular, neurological, retinal and kidney damage over a period of time (Nickerson and Dutta 2012). Though hyperglycemic condition may not be treated, but the increased sugar levels can be restrained through Food and Drug Administration (FDA)-approved chemically synthesized agents like biguanides, rDNA technology, sulfonylureas and natural extracts (Barwal et al. 2013). Metabolic complications and abnormalities during diabetes arise when reactive oxygen species are generated through activation of a number of pathogenic pathways. Therefore, an increased oxidative stress is observed when the defense system is unable to eliminate excess molecular oxygen or reactive oxygen species (ROS) production during normal oxidative metabolism (Volpe et al. 2018). Hyperglycemia induces generation of free radicals, thus maintaining oxidative stress conditions contributing to

✉ Qayyum Husain
qayyumbiochem@gmail.com

[1] Department of Biochemistry, Aligarh Muslim University, Aligarh, India

[2] Department of Zoology, Aligarh Muslim University, Aligarh, India

Springer

damage of organs and progression in complications of diabetes. Insulin resistance and treatment side-effects such as brain atrophy, fatty liver and anorexia nervosa are some of the numerous limitations of insulin therapy during diabetes management (Niedowicz and Daleke 2005). This creates a need of an economic and equally effective therapeutic agent able to control oxidative stress induced by hyperglycemic condition, to forge a breakthrough in treatment of diabetes mellitus.

The nanosized particles have fascinated improvement in activity of healthcare products and drugs. A number of nanosized drugs are being synthesized to target specific diseases due to availability of their large surface area-binding drug molecules or their in-built mechanism as controlling agents. FDA has approved many nanodrugs by different pharmaceutical companies that have been tried and tested for their functional ability to treat diseases and replace conventional drug formulations (Jones et al. 2018). Since 1995, more than 50 nanodrugs have been approved by FDA which can be administered orally and intravenously, and are currently available for clinical use. Most of the nanodrugs that have been approved for clinical use have shown reduced toxicity with improved efficacy. Doxil by Janssen has been approved for Karposi's sarcoma and ovarian cancer due to its increased delivery specificity to the target site and reduced toxicity. Protein based Abraxane by Celgene is approved for breast and pancreatic cancer with greater solubility and increased delivery to tumor site. Inorganic nanoparticles-based drugs like Feraheme by AMAG have been approved by FDA for treatment of iron deficiency in chronic kidney disease owing to its prolonged and steady release with frequent dosing. These nanoformulations are now undergoing clinical trials showing promising results in treatment of various diseases (Ventola 2017). Recently, inorganic nanoparticles (NPs) have garnered tremendous attention in different biomedical fields as a low-cost and non-toxic nanomaterial. Inorganic NPs have potential as antibacterial, anticancer, antioxidant, anti-inflammatory, immobilization agents suitable for drug delivery and other industrial purposes (Husain 2018; Ansari and Husain 2012; Gaillet and Rouanet 2015; Ahmed et al. 2018; Ahmed and Husain 2019). It has been shown that zinc oxide NPs (ZnO NPs) actively present significantly high genotoxicity and cytotoxicity against cancer cells through apoptotic cell induction by ROS-generated mitochondrial pathway (Sharma et al. 2012). The regulatory action of autophagy and its link with ROS in ZnO NP-treated lung epithelial cells demonstrated impairment of autophagic flux and accumulation of autophagosomes in A549 cells by the ZnO NPs (Zhang et al. 2017). Surface-modified ZnO NPs have been used with different biological molecules functionalized on their surface improving their selectivity and stability against specific cancer cells (Kamaly et al. 2012). ZnO NPs are able to generate excess ROS such as hydroxyl

radicals, hydrogen peroxide and superoxide anion acting as main mechanisms for maintaining toxicity in bacterial cells thus leading to bacterial protein damage and cell membrane disintegration, resulting in bacterial cell death (Zhang and Xiong 2015). The protein expressions of COX-2, TNF-α, IL-1β, IL-6 and iNOS with nitrogen oxide (NO) production are suppressed in a dose-dependent manner by ZnO NPs exhibiting anti-inflammatory activity (Nagajyothi et al. 2015). Evidences have suggested traditional role of Zn as antioxidant, therefore, an in-depth analysis of restorative effects of ZnO NPs in hyperglycemic and oxidative stress conditions is required. We have previously highlighted importance of ZnO NPs in immobilization through simple yet effective procedures of immobilization of β-galactosidase on ZnO NPs and concanavalin A-coated ZnO NPs using adsorption methods (Ansari et al. 2011; Husain et al. 2011).

β-Galactosidase, or lactase, hydrolyzes β-1,4-D galactoside bonds into simpler products such as glucose and galactose from lactose which is markedly present in plants, animals and microorganisms (Husain 2010). β-Galactosidase helps in digestion of milk and milk-products by lactose-intolerant people, thus providing industrial relevance to the enzyme (Haider and Husain 2007) Determination of lactose presence, monitoring gene transcription and activation and conjugation with streptavidin in enzyme-linked immunosorbent assay (ELISA) systems are some of the few important industrial applications of this enzyme (Haider and Husain 2009). Due to exemplar relevance of this enzyme, it was utilized in synthesizing, reducing and capping ZnO NPs in the current study. The ZnO NPs were then characterized with effectiveness of these biologically synthesized ZnO NPs being evaluated on the oxidative stress and biochemical parameters induced by hyperglycemic conditions in streptozotocin (STZ)-treated mice.

## Materials and methods

### Synthesis of ZnO NPs

For synthesizing ZnO NPs, one-pot synthesis method was used, during which 10 mL of 20 mM zinc acetate [Zn(OAc)$_2$·2H$_2$O] was dropwise added to a 10 mL β-galactosidase solution (prepared in sodium acetate buffer, 0.1 M, pH 4.5). The reaction mixture was stirred using magnetic stirrer at room temperature for 5 h. Then 10 mL 20 mM NaOH was added dropwise to the mixture till the pH reached 12. The precipitate was re-dispersed in deionised water thrice and centrifuged. Finally, the obtained white powder was dried in an oven overnight at 50 °C. The final product in the form of ZnO NPs was obtained in the form of dried white powder that was used for further characterization and in vivo experimentation.

## Characterization of ZnO NPs

Different spectroscopic and microscopic techniques were involved in characterization of enzymatically synthesized ZnO NPs. UV–Vis spectra were obtained on UV-1800 (Shimadzu, Japan) UV–Vis spectrophotometer in the wavelength range of 250–500 nm. Transmission electron micrographs (TEM) were obtained on JEM 2100 (JEOL, Japan) transmission electron microscope. DynaPro-TC-04 dynamic light scattering equipment (Proteins Solutions, Wyatt Technology, Santa Barbara, CA, USA) was used to perform dynamic light spectroscopy (DLS) at an average rate of 10 scans at 25 °C. The X-ray diffraction analysis of phase structure of ZnO NPs was obtained using Rigaku Miniflex-II (Japan) X-ray diffractometer (XRD) at intensity of 20°–80° with 4 cycles s$^{-1}$ of scan speed via X-ray monochromatic beam. Fourier transform infrared spectroscopy (FTIR) was performed using Perkin Elmer FTIR instrument (USA) from 4000 to 400 cm$^{-1}$ by the potassium bromide (KBr) pellet method to analyze the existence of various vibrational modes.

## Selection of experimental animals

Thirty six male albino mice (6 months in age, 20–25 g) were obtained from Animal House (Jamia Hamdard University, New Delhi, India). The temperature was maintained at around 25 °C under 12 h-day/12 h-night cycles, respectively. Standard dietary pellets and clean water were made accessible to the mice and they were acclimatized for 15 days in sheltered aseptic conditions in compliance to the guidelines of Departmental Ethical Committee for Animal Experimentation, Department of Biochemistry, AMU, Aligarh, India.

## Induction of diabetes and treatment with ZnO NPs

A single intraperitoneal dose of STZ (120 mg kg$^{-1}$ body weight) was mixed in sodium citrate buffer (50 mM, pH 4.5) with further dissolution of 0.1 M sodium chloride and administered to mice for induction of diabetes. The fasting blood glucose level was estimated after 7 days through peripheral blood withdrawn from tail vein of mice. Following induction of diabetes, 36 mice were divided into 6 groups with 6 mice in each group, and were characterized as follows: Group I: normal healthy mice as untreated control (C); Group II: diabetic control mice (DC); Group III: normal healthy mice treated with ZnO NPs (NC, 2 mg kg$^{-1}$ body weight week$^{-1}$); Group IV: diabetic mice treated with ZnO NPs (NT1, 0.5 mg kg$^{-1}$ body weight week$^{-1}$); Group V: diabetic mice treated with ZnO NPs (NT2, 1 mg kg$^{-1}$ body weight week$^{-1}$), and; Group VI: diabetic ice treated with ZnO NPs (NT3, 2 mg kg$^{-1}$ body weight week$^{-1}$). All

mice groups treated with ZnO NPs were administered the doses using intraperitoneal injections and treated over a time period of 28 days.

## Sample preparation

Following the experimental period, animals were fasted overnight, then euthanized using cervical dislocation. Blood samples were immediately collected in sterilized tubes containing sodium fluoride for ascertaining fasting blood glucose levels. The tubes were centrifuged at 3000×$g$ for 10 min using cooling centrifuge. Sera and plasma were segregated in Eppendorf tubes and stored at − 20 °C for further experimentation. Tissue samples of liver, kidney and pancreas were removed and stored in Hepes buffer at − 20 °C for histopathological studies. The sacrifice was carried out in accordance to the DECAE, Department of Biochemistry, AMU (India) towards human care for experimental animals.

## Estimation of changes in body weight and glucose levels

Each mice from different groups were weighed for their estimated changes in body weight at weekly intervals. Oxidase–peroxidase method was utilized for estimating fasting blood glucose levels (Trinder 1969). Horseradish peroxidase (6.2 U mL$^{-1}$), glucose oxidase (6.7 U mL$^{-1}$), phosphate buffer (8 M), 4-aminoantipyrine (0.2 mM) and phenol (86 mM) were added to fasting blood samples to make working solutions. Standard glucose solution (100 mg dL$^{-1}$) and deionized water was added to the working solution to prepare blank and standard solutions. All the solutions were mixed thoroughly and incubated at room temperature for 30 min. Finally, the absorbance at wavelength 505 nm was recorded. 3% trichloroacetic acid was mixed in serum samples in a ratio of 1:3 and centrifuged at 3000×$g$ for 10 min for deproteination.

## Estimation of carbohydrate metabolic enzymes

For determining activity of lactate dehydrogenase (LDH), time-dependent decrease in absorbance due to oxidation of NADH was measured at 340 nm for 5 min at room temperature by the methods described previously by Kornberg (1955). Fructose-1,6-bisphosphatase (FBPase) and glucose-6-phosphatase (G6Pase) activities were measured at 37 °C through release of inorganic phosphate from fructose-1,6-biphosphate and glucose-6-phosphate as described by Freeland and Harper (1959) and Shull et al. (1956), respectively. The activities of glucose-6-phosphate dehydrogenase (G6PDH) were measured as time-dependent increment in absorbance at 340 nm for 5 min at room temperature as described by Shonk and Boxer (1964). In each preparation, kidney, liver

and pancreas tissues from two mice from each group were pooled so in all 12 mice were taken.

## Estimation of protein carbonylation, lipid peroxidation, and lipid profile

Lipid peroxidation was assessed by the estimation procedure of Buege and Aust (1978). Malondialdehyde (MDA) is the primary product of peroxidation of lipids and therefore the estimated levels were calculated in nmoles of MDA mg$^{-1}$ of protein (molar extinction coefficient is $1.56 \times 10^{-1}$ M$^{-1}$ cm$^{-1}$). Protein oxidation was estimated with total carbonyl content (molar absorption coefficient is $22 \times 10^3$ M$^{-1}$ cm$^{-1}$) as end-product of oxidation (Levine et al. 1994). The serum lipid profile (cholesterol, triglycerides and HDL-C) was estimated using semi-automated chemistry analyzer (Lab-Life Chem Master) on the sample collection day itself.

## Assay of free radical scavengers parameters

### Estimation of non-enzymatic antioxidant parameters

The tissues for estimation of antioxidant parameters were stored in 154 mM NaCl and Tris-Hepes buffer (5 mM, pH 7.5) maintained at − 4 °C. The tissues were then homogenized using Thomas PA glass-Teflon homogenizer (5 pulses, 4 °C). High speed Ultra-Turrex Kunkel homogenizer, Jake & Kunkel GMBH (3 pulses, 30 s intervals) was used for further homogenization of homogenates. The total-SH groups and GSH levels were estimated in the homegenates through yellowish color produced during the reaction with 5,5′-dithiobisnitrobenzoic acid by methods illustrated by Sedlak and Lindsay (1968) and Jollow et al. (1974), respectively. In each preparation, kidney, liver and pancreas tissues from two mice from each group were pooled so in all 12 mice were taken.

### Estimation of enzymatic antioxidant parameters

For superoxide dismutase (SOD) estimation, pyrogallol auto-oxidation methodology by Marklund and Marklund (1974) was utilized, where alteration in absorbance was recorded at 412 nm with specific activity expressed in units mg$^{-1}$ of protein. The activity of catalase (CAT) was estimated by the method proposed by Aebi (1984), where change in absorbance was read at 240 nm for 180 s with activity reported as nmol of $H_2O_2$ exhausted mg$^{-1}$ of protein min$^{-1}$. In each preparation, kidney, liver and pancreas tissues from two mice from each group were pooled so in all 12 mice were taken.

## Estimation of liver and kidney function markers in serum

All estimations were carried forward using the available commercial kit (Span Diagnostics, India). The reaction of DNPH with oxaloacetate was used to estimate aspartate transaminase (AST) by the method of Reitman and Frankel (1957), where the absorbance of brown colored product, hydrazone was read at 505 nm. The reaction of DNPH with pyruvate was used to estimate alanine transaminase (ALT) by similar method with same product as AST estimation measured at 505 nm (Farooqui et al. 2017). The estimation of alkaline phosphatase (ALP) is based on the reaction of phenyl phosphate to give by-products inorganic phosphate and phenol, finally resulting in an orange–red complex after reaction of phenol with potassium ferricyanide (Kind and King 1954). For estimation of urea levels in serum samples, commercially available kit (Span Diagnostics, India) was used. The urea levels were assessed in mg dL$^{-1}$ of the sample.

## Histopathological studies

The histopathological slides of liver, kidney, and pancreas were prepared as per the protocol of Gray (1954) with required modification by Ahmad et al. (2018). After sacrificing the mice, the liver, kidney, and pancreas were taken out, cut into slices and left in Bouin's fluid for 24 h. Then the slices were dehydrated in graded alcohol (30%, 50%, 70%, 90% and absolute alcohol) for 5 min each. The slices were then cleaned by sequential incubation in 70/30% and 30/70% of ethanol/xylene for 5 min each and finally cleaned in xylene for 10 min. The slices were then embedded in mixture of paraffin and was (3:1). The slices were then cast in blocks and sections of about 5 μm were cut with microtome (Labotech, Rotary type). The section ribbon were then placed over glass slide (rubbed with a layer of glycerin and albumin, 1:1) and placed on a hot plate (40–45 °C). The treatment of slides was carried in xylene for 5 min and further rehydrated with a series of graded alcohol. Finally, the slides were stained in haematoxylin–eosin (H–E) and examined under light microscope (Nikon, Japan).

## Ethical statement for animal experimentation

The experimentation on animals was permitted by Ministry of Environment, Forests and Climate Change, Government of India under registration number 714/GO/Re/S/02/CPCSEA issued by Committee for the Purpose of Control and Supervision of Experiments on Animals (CPCSEA) and authorized by the Institutional Animal Ethic Committee (IAEC) of Department of Biochemistry, Faculty of Life Sciences, Aligarh Muslim University, Aligarh, India.

## Statistical analysis

Statistical evaluation of the experimentation was managed using one-way ANOVA through Origin 8.1 software (USA). Dunnet's multiple comparison post hoc test was used for comparison amongst various groups with $p < 0.05$ being selected as probability indicator of statistical significance. All data were expressed as mean $\pm$ SD for at least three different preparations.

## Results

### Characterization of ZnO NPs

Figure 1a records the UV–Vis absorption spectrum of β-galactosidase-mediated synthesized ZnO NPs over a varying period of time for 5 h. The prominent and distinct peak

centered at 376 nm specifically illustrates the time-dependent synthesis of ZnO NPs that occurs due to the enhanced excitation binding energies. As the duration of reaction time increases, the $Zn^{2+}$ ions transform their oxidation state towards more stable $Zn^0$ state. The band gap increases for absorption spectroscopy when the particle size decreases. The wavelength of absorption and the band gap possess an opposing ratio. TEM micrograph reveals spherical clusters of ZnO NPs with size of NPs around 20–24 nm (Figs. 1b, S1). The size of the NPs was further confirmed using DLS analysis which displayed an average size of 21.9 nm (Fig. S2). XRD pattern of enzyme-mediated synthesized ZnO NPs clearly indicate crystalline structured morphology (Fig. 1c). There were sharp diffraction peaks at $2\theta$ value of 31.85°, 34.5°, 36.3°, 47.55°, 56.45°, 63.1°, and 68.05° with indexing diffraction lattice planes at (100), (002), (101), (102), (110), (103), and (112), respectively, confirming quasi-spherical structure for the synthesized ZnO NPs. The pattern follows
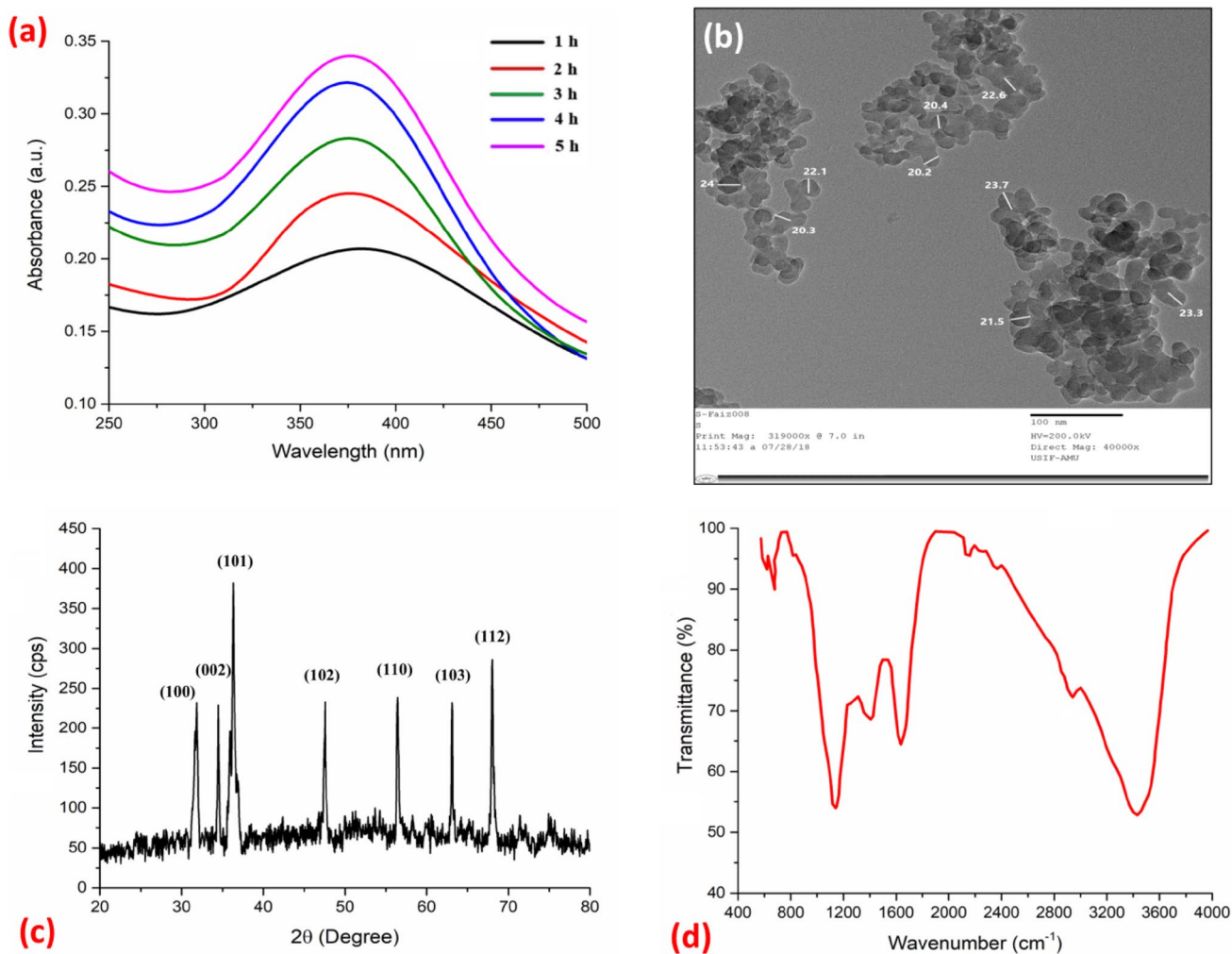


**Fig. 1** **a** UV–Visible spectra analysis of ZnO NPs using ß-galactosidase as a function of time from 1 to 5 h, **b** transmission electron microscope images of ZnO NPs at 100 nm, **c** X-ray diffraction pattern of powdered ZnO NPs, **d** FTIR spectral analysis of ZnO NPs

the standard peaks set by the International Centre for Diffraction Data accordingly.

FTIR spectrum of the synthesized ZnO NPs is provided in Fig. 1d. FTIR is carried forward to confirm the nature and purity of ZnO NPs with the bonds formed during formation of NPs. The peaks that were analyzed at 1634 $cm^{-1}$ confirm the peptide bond linkage and bending of N–H bond between tertiary amines that may be present due to the enzyme capping of the NPs. The peak 600 $cm^{-1}$ corresponds to Zn–O stretching vibration while the peak around 1100 $cm^{-1}$ corresponds to the C–O stretching and bending. There are peaks between 600 and 400 $cm^{-1}$ generated by metal oxides while O–H stretching vibration is indicated by the broad peak at about 3400 $cm^{-1}$.

## Effect of ZnO NPs on changes in body weight and glucose levels of mice

The administration of STZ led to significant loss of weight in diabetic mice. However, dosing with ZnO NPs induced weight gain in diabetic mice reducing cachexia condition significantly (Fig. 2a). The glucose levels have significantly high concentrations in STZ-treated diabetic mice in comparison to control mice (Fig. 2b). After treatment with ZnO NPs, the glucose levels were restored in glycemic mice indicating hypoglycemic effect of ZnO NPs.

## Effect of ZnO NPs on carbohydrate metabolic enzymes

The effect of ZnO NPs alone and their treatment on STZ-induced diabetic mice was assessed on activities of different carbohydrate metabolic enzymes (Table 1). STZ treatment caused significant enhancement in the activity of LDH, an anaerobic glycolysis marker with + 37.30%, + 44.18%, and + 41.46% increment in kidney, liver and pancreatic tissues of diabetic mice, respectively. The treatment of ZnO NPs prevented alterations in LDH by + 7.25%, + 13.95%, and + 20.83% in kidney, liver and pancreas of ZnO NP-treated diabetic mice (2 mg $kg^{-1}$ body weight $week^{-1}$), respectively. The marker enzymes for gluconeogenesis, G6Pase (− 55.31%, − 42.85%, and − 84.61%) and FBPase (+ 54.13%, + 126.02%, and + 89.58%) activities altered in kidney, liver, and pancreas when diabetes was induced in STZ-treated mice. ZnO NP-treated mice (2 mg $kg^{-1}$ body weight $week^{-1}$) ameliorated the alterations in activities of G6Pase (− 12.76%, − 14.28%, and − 38.46%) and FBPase (+ 18.04%, + 49.31%, and + 22.91%) in kidney, liver and pancreas, respectively. There was significant decrease in activities of G6PDH (− 56.29%, − 60.0%, and − 61.66%) in kidney, liver and pancreas of diabetic mice, respectively, which provides NADPH required for anabolic reactions. Administration of increasing concentrations of ZnO NPs
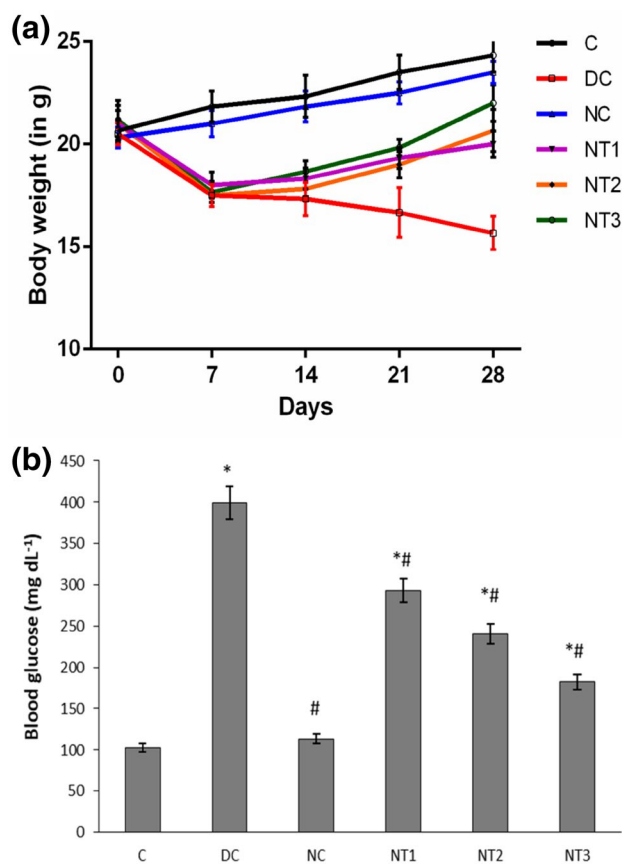


**Fig. 2 a** Body weight changes in mice groups over a period of 28 days, and **b** representative bar graph showing levels of fasting blood glucose after a time period of 28 days. C is control group, DC is STZ-treated diabetic control group, NC is 2 mg $kg^{-1}$ body weight ZnO NP-treated control group, NT1 is 0.5 mg $kg^{-1}$ body weight, NT2 is 1 mg $kg^{-1}$ body weight and NT3 is 2 mg $kg^{-1}$ body weight of ZnO NPs of diabetic treated group of mice, respectively. Results represented are mean ± SD of three independent treatments for all mice in each group. *Significantly different from control at $p \leq 0.05$. #Significantly different from diabetic group at $p \leq 0.05$

(2 mg $kg^{-1}$ body weight $week^{-1}$) increased activity of G6PDH (− 28.88%, − 20.0%, and − 34.16%) in kidney, liver and pancreas, respectively, signifying ameliorating effects of NPs on the carbohydrate metabolic enzymes.

## Effect of ZnO NPs on lipid peroxidation, protein carbonylation and lipid profile

Final products of lipid peroxidation and protein carbonylation estimation, i.e., MDA and carbonyl content levels are assessed for control, diabetic and NP-treated mice. There was a sharp increment in lipid peroxidation in liver, kidney and pancreas when STZ-treatment dosing was performed on the animals (Fig. 3a). There was 53.10% recovery in liver while 57.30% and 46.44% recovery occurred in kidney and pancreas on treatment of diabetic mice with ZnO NPs (2 mg

**Table 1** Effect of ZnO NPs with and without STZ treatment on carbohydrate metabolic enzyme parameters in homogenates

| Groups | Tissues | LDH ($\mu$mol mg$^{-1}$ protein h$^{-1}$) | FBPase ($\mu$mol mg$^{-1}$ protein h$^{-1}$) | G6Pase ($\mu$mol mg$^{-1}$ protein h$^{-1}$) | G6PDH ($\mu$mol mg$^{-1}$ protein h$^{-1}$) |
|---|---|---|---|---|---|
| C | Kidney | $1.93 \pm 0.07$ | $1.33 \pm 0.06$ | $0.47 \pm 0.04$ | $0.135 \pm 0.011$ |
| | Liver | $0.43 \pm 0.04$ | $0.73 \pm 0.05$ | $0.21 \pm 0.016$ | $0.035 \pm 0.004$ |
| | Pancreas | $0.24 \pm 0.03$ | $0.48 \pm 0.03$ | $0.13 \pm 0.042$ | $0.24 \pm 0.022$ |
| NC | Kidney | $1.95 \pm 0.08^{\#}$ | $1.3 \pm 0.07^{\#}$ | $0.43 \pm 0.05^{\#}$ | $0.119 \pm 0.02^{\#}$ |
| | Liver | $0.44 \pm 0.04^{\#}$ | $0.78 \pm 0.05^{\#}$ | $0.24 \pm 0.018^{\#}$ | $0.03 \pm 0.008^{\#}$ |
| | Pancreas | $0.27 \pm 0.03^{\#}$ | $0.41 \pm 0.03^{\#}$ | $0.15 \pm 0.02^{\#}$ | $0.215 \pm 0.03^{\#}$ |
| DC | Kidney | $2.65 \pm 0.08^{*}$ | $2.05 \pm 0.09^{*}$ | $0.25 \pm 0.03^{*}$ | $0.059 \pm 0.05^{*}$ |
| | Liver | $0.62 \pm 0.05^{*}$ | $1.65 \pm 0.06^{*}$ | $0.12 \pm 0.023^{*}$ | $0.014 \pm 0.003^{*}$ |
| | Pancreas | $0.41 \pm 0.04^{*}$ | $0.91 \pm 0.05^{*}$ | $0.02 \pm 0.015^{*}$ | $0.092 \pm 0.007^{*}$ |
| NT1 | Kidney | $2.44 \pm 0.06^{*\#}$ | $1.98 \pm 0.08^{*}$ | $0.29 \pm 0.03^{*}$ | $0.071 \pm 0.004^{*\#}$ |
| | Liver | $0.57 \pm 0.06^{*\#}$ | $1.47 \pm 0.07^{*\#}$ | $0.14 \pm 0.021^{*}$ | $0.021 \pm 0.005^{*\#}$ |
| | Pancreas | $0.37 \pm 0.03^{*}$ | $0.82 \pm 0.04^{*\#}$ | $0.03 \pm 0.012^{*}$ | $0.113 \pm 0.032^{*\#}$ |
| NT2 | Kidney | $2.28 \pm 0.09^{*\#}$ | $1.72 \pm 0.07^{*\#}$ | $0.34 \pm 0.04^{*\#}$ | $0.084 \pm 0.05^{*\#}$ |
| | Liver | $0.52 \pm 0.05^{*\#}$ | $1.25 \pm 0.05^{*\#}$ | $0.15 \pm 0.02^{*\#}$ | $0.023 \pm 0.006^{*\#}$ |
| | Pancreas | $0.32 \pm 0.04^{*\#}$ | $0.66 \pm 0.04^{*\#}$ | $0.06 \pm 0.014^{*\#}$ | $0.136 \pm 0.044^{*\#}$ |
| NT3 | Kidney | $2.07 \pm 0.07^{*\#}$ | $1.57 \pm 0.09^{*\#}$ | $0.41 \pm 0.05^{*\#}$ | $0.096 \pm 0.07^{*\#}$ |
| | Liver | $0.49 \pm 0.04^{*\#}$ | $1.09 \pm 0.06^{*\#}$ | $0.18 \pm 0.019^{\#}$ | $0.028 \pm 0.009^{*\#}$ |
| | Pancreas | $0.29 \pm 0.03^{*\#}$ | $0.59 \pm 0.05^{*\#}$ | $0.08 \pm 0.03^{*\#}$ | $0.158 \pm 0.03^{*\#}$ |

*LDH* lactate dehydrogenase, *G6Pase* glucose-6-phosphatase, *FBPase* fructose-1,6-bisphosphatase, *G6PDH* glucose-6-phosphatase dehydrogenase, *C* control group, *DC* STZ-treated diabetic control group, *NC* 2 mg kg$^{-1}$ body weight ZnO NP-treated control group, *NT1* 0.5 mg kg$^{-1}$ body weight, *NT2* 1 mg kg$^{-1}$ body weight, *NT3* 2 mg kg$^{-1}$ body weight of ZnO NPs of diabetic treated group of mice, respectively. Results represented are mean $\pm$ SD of three independent treatments. In each preparation tissue from two mice from each group was pooled so in all 12 mice were taken. *Significantly different from control at $p \leq 0.05$. #Significantly different from diabetic group at $p \leq 0.05$

kg$^{-1}$ body weight week$^{-1}$). Similarly, there was enhancement in carbonyl content in organs of diabetic mice but treatment with ZnO NPs (2 mg kg$^{-1}$ body weight week$^{-1}$) effectively brought down the levels by 55.43%, 52.17% and 57.54% in liver, kidney and pancreas, respectively (Fig. 3b). The lipid profile (cholesterol, triglycerides and HDL-C) is a significant factor in secondary complications of diabetes (Fig. 3c). There was decrease in HDL-C levels in diabetic mice while cholesterol and triglyceride levels were highly intensified in diabetic mice as compared to the control mice. Dosing with ZnO NPs the lipid profile markers were restored to their normal levels.

## Effect of ZnO NPs on STZ-induced alterations in antioxidant defense parameters

Assessment of ZnO NPs' treatment in STZ-induced oxidative stress is an essential requirement, where effects of concentration-dependent dosing of STZ-treated diabetic mice were observed on different non-enzymatic and enzymatic parameters of oxidative stress defense parameters (Table 2). Treatment of STZ in mice caused enhancement in lipid peroxidation, therefore, there was marked decrease in total-SH ($-32.82\%$, $-22.57\%$, and $-47.17\%$) and GSH

($-83.66\%$, $-44.32$, and $-70.76\%$) in kidney, liver and pancreas tissue activities, respectively. Treatment of ZnO NPs regulated and reduced the decline in total-SH ($-14.81\%$, $-7.50\%$, and $-16.12\%$) and GSH ($-18.25\%$, $-13.40\%$, and $-24.61\%$) activities in kidney, liver and pancreas, respectively. STZ treatment caused marked decrease in activities of enzymatic antioxidant parameters, like SOD ($-47.09\%$, $-30.41\%$, and $-43.52\%$) and CAT ($-40.73\%$, $-52.01\%$, and $-44.91\%$), while ZnO NPs administration following STZ-treatment, prevented STZ-induced decline in activities of these antioxidant enzyme parameters, viz, SOD ($-14.68\%$, $-13.25\%$, and $-13.87\%$) and CAT ($-8.97\%$, $-22.20\%$, and $-20.44\%$) in kidney, liver and pancreas, respectively, in treated animals.

## Effect of ZnO NPs on liver and kidney function markers

Liver function is represented by levels of enzymes ALT, AST, and ALP in serum samples (Fig. 4a). The diabetic groups showed increased levels of ALT, AST, and ALP with dose-dependent decrease when these groups were dosed with ZnO NPs. The higher dosed ZnO NPs group (2 mg kg$^{-1}$ body weight week$^{-1}$) showed significant recovery in these
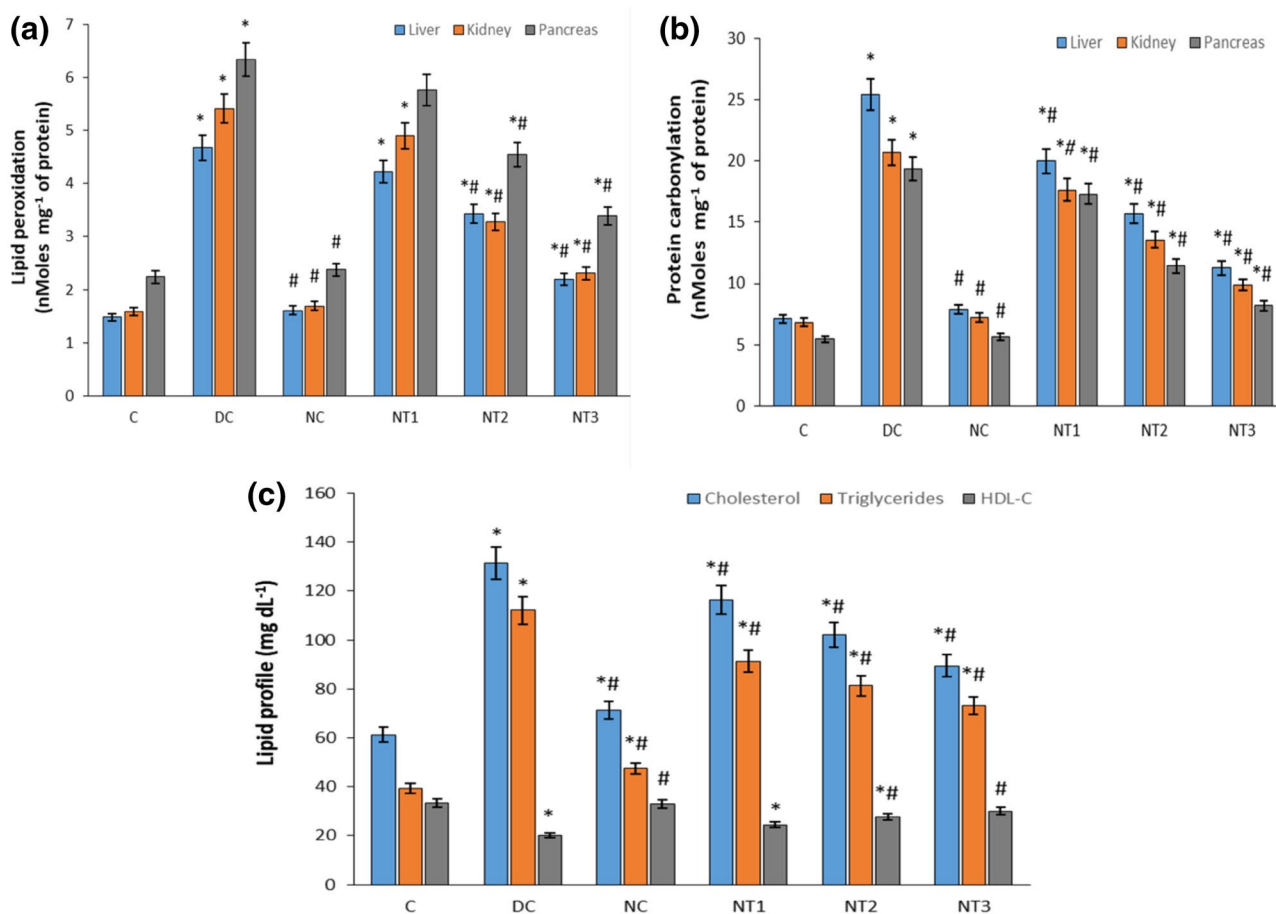
**Fig. 3** **a–c** Lipid peroxidation, carbonyl contents and lipid profile in liver, kidney and pancreas of normal, diabetic, ZnO NP-supplemented normal and ZnO NP-treated diabetic group of mice, respectively. C is control group, DC is STZ-treated diabetic control group, NC is 2 mg $kg^{-1}$ body weight ZnO NP-treated control group, NT1 is 0.5 mg $kg^{-1}$ body weight, NT2 is 1 mg $kg^{-1}$ body weight and NT3 is 2 mg $kg^{-1}$ body weight of ZnO NPs of diabetic-treated group of mice, respectively. Results represented are mean ± SD of three independent treatments for all mice in each group. *Significantly different from control at $p \leq 0.05$. #Significantly different from diabetic group at $p \leq 0.05$

marker levels. Kidney function is represented by alterations in urea levels in serum (Fig. 4b). The diabetic groups possessed higher urea levels as compared to control group. ZnO NPs supplemented groups showed significant improvement in urea levels.

## Histopathological observations of treatment with ZnO NPs

### Histopathological analysis of liver

In the normal liver (control group), the photomicrograph showed normal histological features of hepatocytes with single plate-thick hepatocytes and normal central vein hepatocytes are regular having sizeable spheroidal nucleus and distinctly marked nucleolus (Fig. 5a). The ZnO NP-treated liver samples also showed almost normal histological architecture of the tissue with mild vacuolated degeneration in the hepatocytes (Fig. 5b). The diabetic liver samples showed marked distortion in the histological architecture of the liver tissue. The photomicrograph showed areas of necrosis, congested portal vein, foci of degenerated hepatocytes with intensely eosinophilic cytoplasm, focal collection of inflammatory cells as well as marked pigment deposition in the parenchyma (Fig. 5c). Interestingly, treatment of ZnO NPs to the diabetic mice restores the normal architecture of the liver to a greater extent in a dose-dependent manner. The tissues of diabetic mice treated with ZnO NPs (0.5 mg $kg^{-1}$ body weight) showed least amelioration as marked vacuolar degeneration of hepatocytes was observed along with perivenular fibrosis (Fig. 5d). The diabetic mice treated with ZnO NPs (1 mg $kg^{-1}$ body weight) showed mild-to-moderate vacuolar degeneration of hepatocytes with fat cysts and foci of necrosis (Fig. 5e). However, the diabetic mice treated with ZnO NPs (2 mg $kg^{-1}$ body weight) showed maximum restoration of liver tissue architecture with only

**Table 2** Effect of ZnO NPs with and without STZ treatment on enzymatic and non-enzymatic parameters in homogenates

| Groups | Tissues | Total-SH ($\mu$mol g$^{-1}$ tissue) | GSH ($\mu$mol g$^{-1}$ tissue) | SOD (units mg$^{-1}$ protein) | CAT ($\mu$mol mg$^{-1}$ protein min$^{-1}$) |
|---|---|---|---|---|---|
| C | Kidney | $7.83 \pm 0.35$ | $1.09 \pm 0.029$ | $34.4 \pm 2.70$ | $98.21 \pm 4.98$ |
| | Liver | $16.21 \pm 0.63$ | $0.97 \pm 0.037$ | $36.07 \pm 1.85$ | $25.36 \pm 1.05$ |
| | Pancreas | $4.96 \pm 0.24$ | $0.065 \pm 0.002$ | $18.45 \pm 1.64$ | $9.93 \pm 0.99$ |
| NC | Kidney | $7.90 \pm 0.27^{\#}$ | $1.13 \pm 0.035^{\#}$ | $35.19 \pm 2.54^{\#}$ | $104.72 \pm 4.76^{\#}$ |
| | Liver | $16.78 \pm 0.58^{\#}$ | $1.04 \pm 0.03^{\#}$ | $36.9 \pm 1.68^{\#}$ | $24.78 \pm 2.37^{\#}$ |
| | Pancreas | $5.09 \pm 0.25^{\#}$ | $0.07 \pm 0.002^{\#}$ | $19.23 \pm 1.52^{\#}$ | $9.12 \pm 1.02^{\#}$ |
| DC | Kidney | $5.26 \pm 0.49^{*}$ | $0.178 \pm 0.024^{*}$ | $18.2 \pm 1.37^{*}$ | $58.20 \pm 3.15^{*}$ |
| | Liver | $12.55 \pm 0.53^{*}$ | $0.54 \pm 0.042^{*}$ | $25.1 \pm 2.83^{*}$ | $12.17 \pm 1.53^{*}$ |
| | Pancreas | $2.62 \pm 0.17^{*}$ | $0.019 \pm 0.001^{*}$ | $10.42 \pm 1.02^{*}$ | $5.47 \pm 0.83^{*}$ |
| NT1 | Kidney | $5.45 \pm 0.31^{*\#}$ | $0.457 \pm 0.026^{*\#}$ | $22.95 \pm 1.74^{*\#}$ | $67.42 \pm 3.65^{*\#}$ |
| | Liver | $13.12 \pm 0.67^{*\#}$ | $0.67 \pm 0.043^{*\#}$ | $27.81 \pm 1.95^{*\#}$ | $14.84 \pm 1.09^{*\#}$ |
| | Pancreas | $2.98 \pm 0.28^{*\#}$ | $0.028 \pm 0.002^{*\#}$ | $13.93 \pm 2.13^{*\#}$ | $6.56 \pm 1.2^{*\#}$ |
| NT2 | Kidney | $6.17 \pm 0.43^{*\#}$ | $0.673 \pm 0.032^{*\#}$ | $25.46 \pm 1.88^{*\#}$ | $79.05 \pm 3.43^{*\#}$ |
| | Liver | $13.87 \pm 0.72^{*\#}$ | $0.71 \pm 0.039^{*\#}$ | $29.11 \pm 2.2^{*\#}$ | $17.45 \pm 2.49^{*\#}$ |
| | Pancreas | $3.54 \pm 0.13^{*\#}$ | $0.036 \pm 0.002^{*\#}$ | $15.64 \pm 1.95^{*\#}$ | $7.02 \pm 0.94^{*\#}$ |
| NT3 | Kidney | $6.67 \pm 0.0.16^{*\#}$ | $0.891 \pm 0.011^{*\#}$ | $29.35 \pm 1.65^{*\#}$ | $89.40 \pm 4.06^{*\#}$ |
| | Liver | $14.95 \pm 0.69^{*\#}$ | $0.84 \pm 0.038^{*\#}$ | $31.29 \pm 2.76^{*\#}$ | $19.73 \pm 2.31^{*\#}$ |
| | Pancreas | $4.16 \pm 0.2^{*\#}$ | $0.049 \pm 0.003^{*\#}$ | $15.89 \pm 1.45^{*\#}$ | $7.9 \pm 1.67^{*\#}$ |

*SH* thiol group, *GSH* glutathione, *SOD* superoxide dismutase, *CAT* catalase, *C* control group, *DC* STZ-treated diabetic control group, *NC* 2 mg kg$^{-1}$ body weight ZnO NP-treated control group, *NT1* 0.5 mg kg$^{-1}$ body weight, *NT2* 1 mg kg$^{-1}$ body weight, *NT3* 2 mg kg$^{-1}$ body weight of ZnO NPs of diabetic treated group of mice, respectively. Results represented are mean $\pm$ SD of three independent treatments. In each preparation tissue from two mice from each group was pooled so in all 12 mice were taken. *Significantly different from control at $p \leq 0.05$. #Significantly different from diabetic group at $p \leq 0.05$

mild dilated and congested central vein, mild vacuolization of hepatocytes and Kuffer hyperplasia. The cytoplasm of hepatocytes showed a clear appearance without any blurry visualization (Fig. 5f).

### Histopathological analysis of kidney

In the control group, histopathological analysis of kidneys showed typical histological features. The photomicrograph showed normal tubular epithelial cells, normal renal area and glomeruli with regular tufts of capillaries, cortical parenchyma, and surrounded by Bowman's capsule (Fig. 6a). The photomicrograph of ZnO NP-treated kidney also showed almost normal histological architecture of the tissue with normal renal glomeruli with tubular epithelial cells and foci of hyaline casts in the tubular lumen (Fig. 6b). The photomicrograph of diabetic kidney showed marked proliferation of glomerular capillaries with infiltration of lymphocytes. Dense lymphoplasmacytic infiltrate was also seen in the interstitium with focal destruction of renal tubular epithelium (Fig. 6c). However, the diabetic mice treated with ZnO NPs showed restoration of normal architecture of kidney in a dose-dependent manner. The photomicrograph of kidney treated with ZnO NPs (0.5 mg kg$^{-1}$ body weight) showed minimum restoration potential of NPs as marked atrophied

glomerular capillaries with dilated Bowman's space with widespread destruction of tubular epithelial cells lining with hyaline casts in the tubular lumen (Fig. 6d). The photomicrograph of kidney treated with ZnO NPs (1 mg kg$^{-1}$ body weight) showed moderate restoration of kidney architecture as sparse lymphocyte infiltrate in the glomeruli with mild lymphoplasmacytic infiltrate in the interstitium, degeneration of epithelial lining with mild fibrosis was observed (Fig. 6e). Interestingly, the photomicrograph of kidney treated with ZnO NPs (2 mg kg$^{-1}$ body weight) showed maximum restoration as normal architecture of kidney with normal glomerular capillary tufts with hyaline cysts in the lumen of few tubules only (Fig. 6f).

### Histopathological analysis of pancreas

In the control group, the photomicrograph showed normal histological features of pancreatic acini and islet of Langerhans cells (Fig. 7a). The photomicrograph of NP-treated pancreas showed near-normal islet of Langerhans with a close cuff of pancreatic acini around it (Fig. 7b). The photomicrograph of diabetic control group showed contracted and shrunken islet of Langerhans with vascular congestion, and sparse lymphocytic infiltrate. The islet of Langerhans cells nuclei showed mild hyperchromasia with vascular
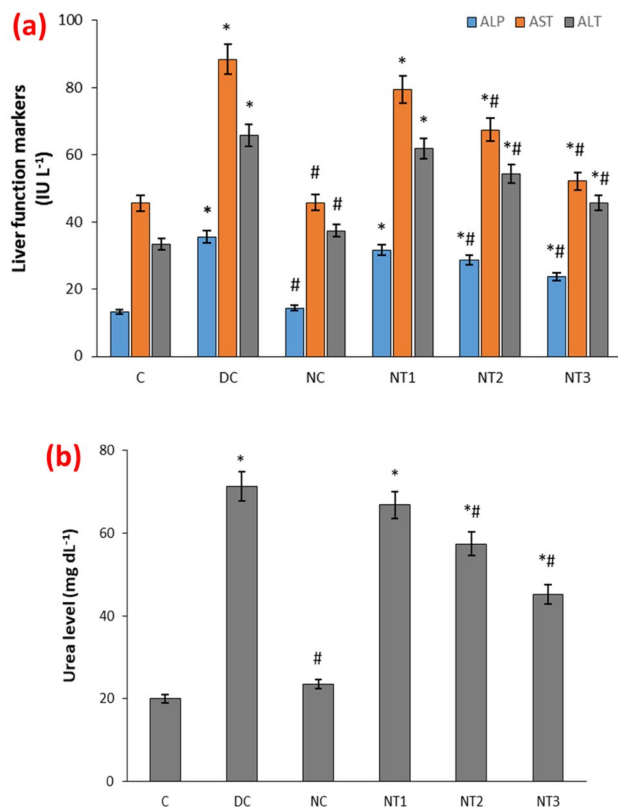
**Fig. 4** **a**, **b** Liver function markers and urea levels in serum. Urea was measured as a kidney function marker and ALT, AST, and ALP were measured as a liver function in serum of normal, diabetic, ZnO NPs supplemented normal and ZnO NP-treated diabetic group of mice, respectively. C is control group, DC is STZ-treated diabetic control group, NC is 2 mg kg$^{-1}$ body weight ZnO NP-treated control group, NT1 is 0.5 mg kg$^{-1}$ body weight, NT2 is 1 mg kg$^{-1}$ body weight and NT3 is 2 mg kg$^{-1}$ body weight of ZnO NPs of diabetic treated group of mice, respectively. Results represented are mean±SD of three independent treatments for all mice in each group. *Significantly different from control at $p \leq 0.05$. #Significantly different from diabetic group at $p \leq 0.05$

degeneration of cytoplasm. Focal atrophy of pancreatic acinar cells was also observed with clear area between islet of Langerhans and acini (Fig. 7c). Interestingly, the treatment of ZnO NP-treated diabetic mice restored the normal architecture of the pancreas to great extent in a dose-dependent manner. The tissue of diabetic mice treated with ZnO NPs (0.5 mg kg$^{-1}$ body weight) showed moderately atrophied islet of Langerhans with vascular degeneration of cytoplasm along with regenerated pancreatic acini. Vascular congestion is also not observed, however, sparse lymphocytes are still noted (Fig. 7d). The diabetic mice treated with ZnO NPs (1 mg kg$^{-1}$ body weight) showed regenerated islet of Langerhans with increase in its diameter, foci of moderate hydropic degeneration, moderate necrosis, and increase in size of β-cells (Fig. 7e). However, the diabetic mice treated with ZnO NPs (2 mg kg$^{-1}$ body weight) showed maximum

restoration of pancreatic architecture with regenerated islet of Langerhans, foci of mild hydropic degeneration, mild necrosis and near normal surrounding pancreatic acini. Size of the β-cells is also near normal (Fig. 7f).

# Discussion

The pharmacokinetic profile of drugs can be modified by extensive use of nanotechnology. The advancement in nanotechnology has made use of NPs in targeted therapy as drugs with improved specificity towards target sites, minimal side-effects and toxicity. These nanodrugs can also influence resistivity of target cells towards conventional drugs. In our study, the focus was on synthesizing biocompatible nanodrug in the form of ZnO NPs using one-pot bio-enzymatic synthesis methodology. Our previous studies have shown prospects of enzymatically synthesized NPs towards in vitro hyperglycemic conditions and therefore it was essential to highlight the action of these NPs in animal model to establish their potential use as nanomedicinal drug. Our results highlight the advantage of supplementation of ZnO NPs to diabetic groups significantly improves the primary and secondary complications due to diabetes and therefore possibility of future use as nanomedicine.

Diabetes is followed by high blood glucose levels characterized by a group of metabolic disorders, being one of most epidemic factors globally causing deaths spanning across all continents. It has been reported that metals like copper, manganese, magnesium, iron, selenium, chromium and zinc play an important part in glucose homeostasis and they are directly associated with deficiency-related implications of diabetes (Meyer and Spence 2009). Amongst these metals, zinc is identified as an essential micronutrient being in association with hundreds of enzymes. The activity of zinc on insulin signaling pathway improves hepatic glycogenesis, thus enhancing utilization of glucose (Jansen et al. 2009). Whenever there is spike in blood glucose levels, insulin is secreted in response by β cells of pancreas. Zinc is the core around which insulin is produced as solid hexamer, therefore establishing direct relationship of zinc with insulin. Also, zinc has been reported to reduce glycogenolysis and gluconeogenesis through inhibition in glucagon secretion (Egefjord et al. 2010). Keeping this property of zinc in mind, ZnO NPs were bio-enzymatically synthesized by β-galactosidase. One-pot simple methodology of NP synthesis was utilized where zinc acetate was precursor and β-galactosidase acted as capping and reducing agent on the NPs. The NPs were characterized using different biophysical and microscopic methods highlighting synthesis of stable sphere-shaped NPs.

The primary indication of induction of diabetes was the weight loss in animals treated with STZ. Due to decreased insulin levels, the blood glucose level also tends to shoot
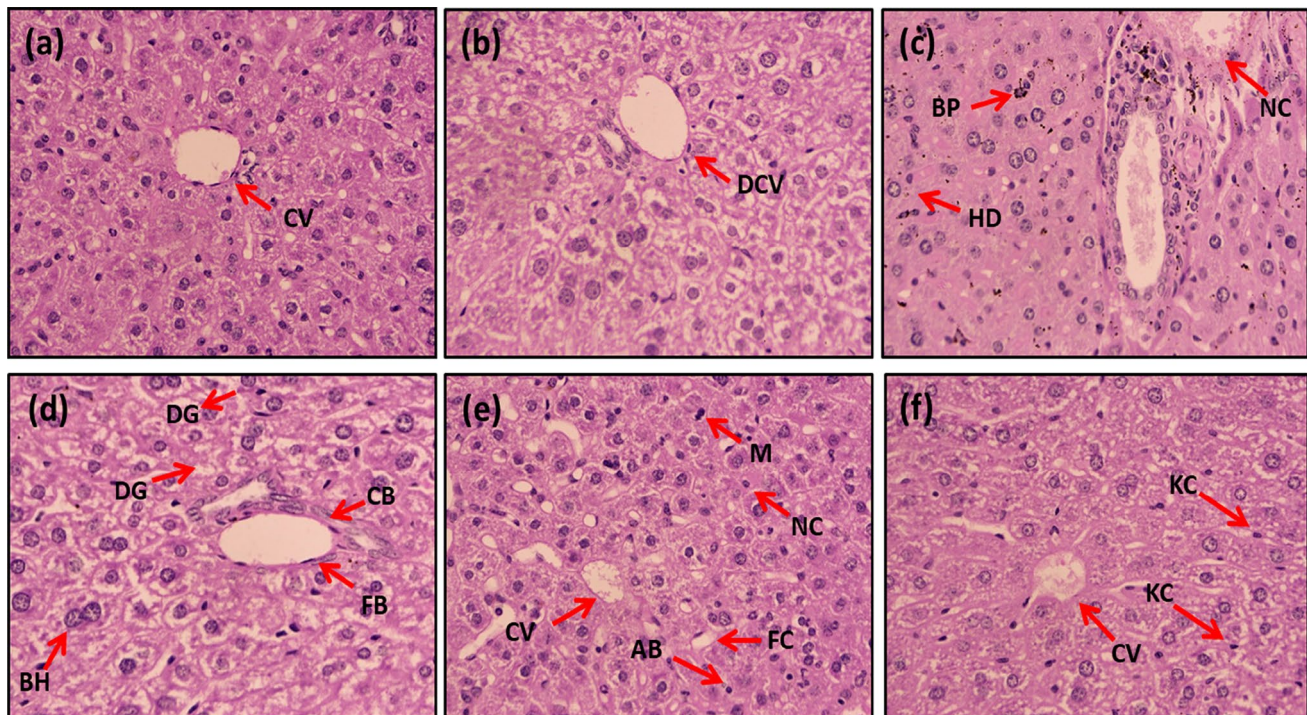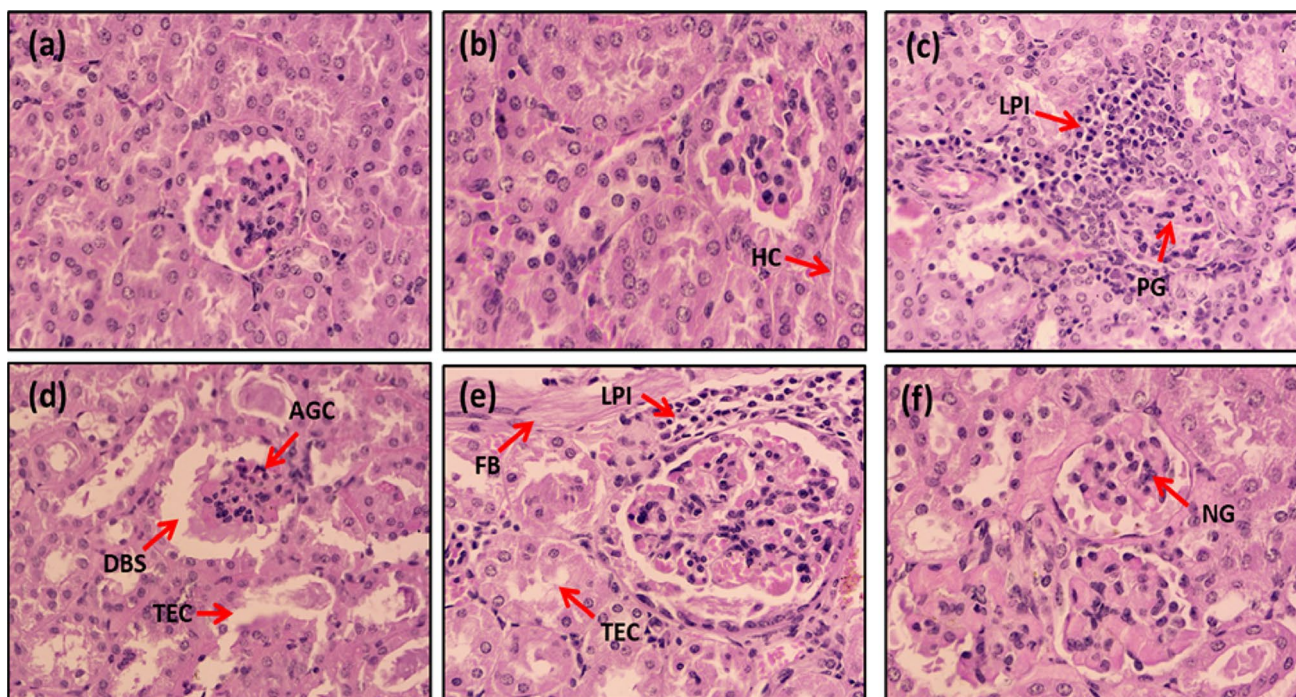
**Fig. 5** Histopathological studies of liver. **a** Normal liver. Photomicrograph showing normal architecture of hepatocytes with single plate-thick hepatocytic cords and normal central vein. **b** Liver treated with NPs (2 mg kg$^{-1}$ body weight ZnO NPs). Photomicrograph showing normal architecture of hepatocytes with mild dilated central vein. **c** Diabetic liver. Photomicrograph showing focal areas of necrosis with congested portal vein. Foci of hepatocytic degeneration with intensely eosinophilic cytoplasm along with bile pigmentation in parenchyma, and **d–f** Liver treated with NPs (0.5, 1, and 2 mg kg$^{-1}$ body weight ZnO NPs). The treatment of NPs to diabetic mice restores the normal histopathological architecture of liver tissue in a dose-dependent manner. Representative images of $n = 3$ for each experimental group are shown. Hematoxylin–eosin staining: ×40; *CV* central vein, *DCV* dilated central vein, *NC* necrosis, *BP* bile pigment, *FB* fibrosis, *BH* binucleated hepatocytes, *HD* hepatocytic degeneration, *DG* degeneration, *M* mitosis, *NC* necrosis, *AB* apoptotic bodies, *FC* fat cysts, *KC* Kupffer cells

up swiftly. It has already been suggested by previous studies that diabetes leads to secondary complications such as increased levels of low-density lipoprotein (LDL) cholesterol and triglycerides with reduction in high-density lipoprotein (HDL) cholesterol since there is reduced cholesterol biosynthesis. These abnormalities in LDL and HDL contribute to development of cardiovascular diseases like atherosclerosis and stroke (Nancy et al. 2006). The results in our study indicated ZnO NPs treatment led to remarkable recuperation in triglyceride and cholesterol levels towards normal. The results confirmed ZnO NPs acted as lipid profile regulator decreasing the imminent cardiovascular risks related to diabetes. These anti-hyperlipidemic effects of ZnO NPs could be associated with stimulating or mimetic insulin-like nature of NPs on the effected pancreatic β cells. ZnO NPs also tend to regulate the carbohydrate metabolic enzymes, thus helping in controlling hyperglycemic condition in the animals. The glycolytic pathway produces lactate with simultaneous oxidation of NADH to NAD$^+$ in the cytoplasm via reduction of pyruvate catalyzed by LDH (Jialal and Sokoll 2015). The levels of lactate significantly increase in diabetic conditions due to overexpression of LDH. The enzymatic activity is ameliorated by ZnO NPs leading to proper functioning of these cycles. The activities of FBPase and G6Pase have importance as contributors towards increment in free blood glucose through gluconeogenesis pathway. Hyperglycemic state during diabetes curbs activities of these enzymes leading to disrupted glucose equilibria. ZnO NPs enhanced activities of these enzymes in diabetic groups of mice indicating beneficial effects of the NPs. STZ treatment lead to reciprocal activities of G6PDH, which generate NADPH required for many biosynthetic reactions (Seo et al. 2008). G6PDH deficiency may also lead to red blood cell breakdown causing anemia and jaundice apart from having an important role in NADPH generation. ZnO NPs tend to increase G6PDH activity, and through this there is compensation in activities of both these enzymes through reciprocal effect. Thus, STZ-induced alterations in carbohydrate metabolism were significantly restored towards control on administration of ZnO NPs to the animals.

Hyperglycemia has been implicated with several co-factors such as increased oxidative stress through generation
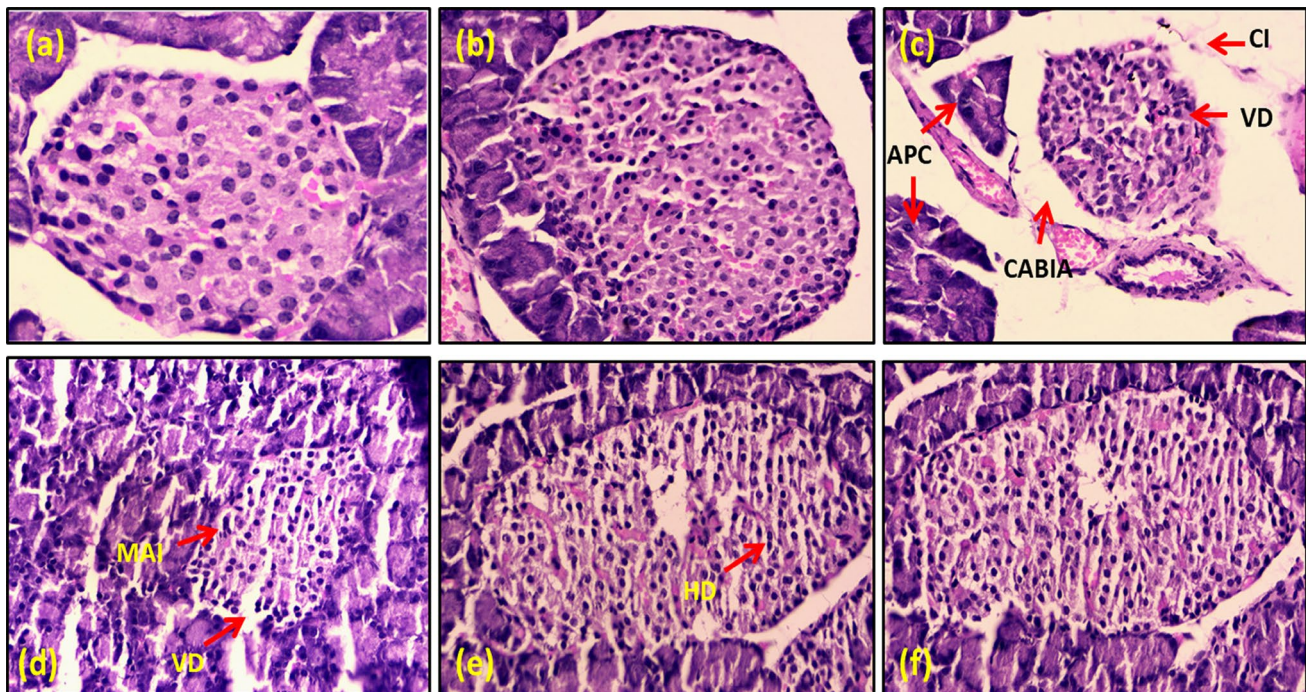
**Fig. 6** Histopathological studies of kidney. **a** Normal kidney. Photomicrograph showing normal glomeruli containing tufts of regular capillaries and surrounded by Bowmen's capsule and tubular epithelial cells. **b** Kidney treated with NPs (2 mg kg$^{-1}$ body weight ZnO NPs). Photomicrograph showing normal renal glomeruli and tubular epithelial cells with foci of hyaline casts in the tubular lumen. **c** Diabetic kidney. Photomicrograph showing marked proliferation of glomerular capillaries with infiltrate of lymphocytes. Lymphoplasmacytic infiltrate seen in the interstitium with focal destruction of renal tubular epithelium, and **d–f** Kidney treated with NPs (0.5, 1, and 2 mg kg$^{-1}$ body weight ZnO NPs). The treatment of NPs to diabetic mice restores the normal histopathological architecture of kidney tissue in a dose-dependent manner. Representative images of $n = 3$ for each experimental group are shown. Hematoxylin–Eosin staining: ×40; *HC* hyaline casts, *LPI* lymphoplasmacytic infiltrate, *PG* proliferation of glomerular capillaries, *AGC* atrophied glomerular capillaries, *DBS* dilated Bowmann's capsule, *TEC* tubular epithelial cells, *FB* fibrosis, *NG* normal glomerulus

of ROS and free radicals. These generated ROS may have damaging effects on cellular machinery and tissues causing injury to the cells of different important organs (Ferdinando and Brownlee 2010). Treatment of animals with STZ increased lipid peroxidation which indirectly led to depletion the total-SH and GSH levels through initiation of oxidative stress. The depleted levels of total-SH and GSH were elevated through ZnO NPs administration to the hyperglycemic animals. The first line of defense against oxidative stress and ROS is formed by the antioxidant enzymes. STZ-induced diabetes led to severe deterioration in antioxidant defense mechanism marked by sharp decrement in the activities of most enzymes like SOD and CAT (Bathina et al. 2017). The functional-SH groups may bind or oxidize in presence of STZ indicating decrease in activities of SOD and CAT. For proper functioning of CAT, NADPH is essentially required, since CAT is an NADPH-binding enzyme (Valavanidisa et al. 2006). Zinc is also an essential cofactor to SOD activity and therefore supplementation of ZnO NPs during hyperglycemic condition may enhance activity of SOD. ZnO NPs also tend to increase the availability of NADPH and thus enhancing activity of CAT. These results indicate strong involvement of ROS in hyperglycemic condition, thus indicating diabetes having inhibitory effects on the antioxidant defense mechanisms. In contrast, ZnO NPs dosing prevented diabetes-induced expression of oxidative stress parameters via direct free radical scavenging and improving activities of the antioxidant enzymes.

The liver and kidney function marker levels are elevated in diabetic animals due to enhanced gluconeogenesis. Urea levels were high in diabetic animals while ALP, AST, and ALT, biomarkers linked to functionality of liver were also elevated hepatic damage. ROS may cause injury to hepatic tissues thereby causing leakage of these enzymes into the bloodstream (Hartmut and Ramachandran 2011). The potential of ZnO NPs in controlling these biomarker levels illustrates the potential of these NPs as antidiabetic drugs. The histopathological results are in sync with biochemical examinations. The liver, kidney and pancreatic micro-architecture were heavily damaged in case of diabetic mice. The histopathological evidences on ameliorating effects of ZnO NPs of hyperglycemic conditions on tissues of liver, kidney and pancreas indicate restoration of normal architecture of the cells in dose-dependent

**Fig. 7** Histopathological studies of pancreas. **a** Normal pancreas. Photomicrograph showed normal histological features of pancreatic acini and islet of langerhans cells. **b** Pancreas treated with NPs (2 mg kg$^{-1}$ body weight ZnO NPs). Photomicrograph of NP-treated pancreas showed near-normal islet of Langerhans with a close cuff of pancreatic acini around it. **c** Diabetic pancreas. Photomicrograph of diabetic control group showed contracted and shrunken islet of langerhans with vascular congestion, and sparse lymphocytic infiltrate, mild hyperchromasia (islet of Langerhans cells), vascular degeneration of cytoplasm, focal atrophy of pancreatic acinar cells, and clear area between islet of Langerhans and acini, and **d**–**f** pancreas treated with NPs (0.5, 1, and 2 mg kg$^{-1}$ body weight ZnO NPs). The photomicrograph showed treatment of NPs to diabetic mice restores the normal histopathological architecture of pancreatic tissue in a dose-dependent manner. Representative images of $n = 3$ for each experimental group are shown. Hematoxylin–eosin staining: ×40; *CI* contracted islets, *VD* vascular degeneration, *APC* atrophied pancreatic acini, *CABIA* clear area between islet and acini, *MAI* moderately atrophied islets of Langerhans, *HD* hydropic degeneration

mechanism. The restoration may be due to the capability of these NPs to decrease oxidative stress parameters by scavenging for damage-causing ROS. There is mild restoration of architecture of β cells in pancreas, that indicate it may be possible to treat secondary complications of diabetes or reducing the damage caused during diabetic environment. Overall, the NPs can be an excellent medium as potential nanomedicine that are specifically targeted and cause restoration of complications due to diabetes, damage of tissues and antioxidant defense mechanisms. The bio-enzymatically synthesized ZnO NPs are non-toxic and may have beneficial therapeutic effects. Previous studies have indicated role of NPs acting as antioxidants, thus exhibiting their true potential for future medicinal purposes (Valgimigli et al. 2018). Thus, this extensive study successfully portrays the importance of these ZnO NPs as an antioxidant and antidiabetic agent. Once the proper mechanism of action of these NPs is deciphered, designing disease-targeted nanoformulations and their equivalent dosage will not be an ardent task.

## Conclusion

In the current study, an enzymatic synthesis of ZnO NPs was actuated using a physiologically important enzyme, β-galactosidase. The enzyme acted as reducing and capping agent synthesizing stable NPs within range of 20–24 nm. Owing to importance of zinc as an essential micro-nutrient, the potential of these ZnO NPs as antidiabetic agent on STZ-induced diabetic mice was evaluated to indicate importance of modulation and further insight of NPs into nanomedicine. The NPs indicated reduction in elevated glucose levels in comparison to control groups. The NPs when treated alone to healthy control did not show any toxicity or damaging effects, thus displaying non-toxic nature of these green NPs. The ZnO NPs control different biochemical parameters and metabolic enzymes towards their normal state when dosed to diabetic mice. Also, the oxidative stress parameters and ROS were drastically reduced proving inhibitory effects of the NPs towards

hyperglycemic secondary complications. The histopathological examinations indicated restoration of normal architecture in ZnO NP-treated diabetic mice thus highlighting potential of these NPs as base for further studies on development of nanodrugs that can be used commercially in place of conventional drugs in the near future.

## Compliance with ethical standards

**Conflict of interest** The authors declare they have no conflict of interest.

## References

Aebi H (1984) Catalase in vitro. Methods Enzymol 105:121–126

Ahmad MF, Ansari MO, Jameel S, Wani AL, Parveen N, Siddique HR, Shadab GGHA (2018) Protective role of nimbolide against chemotherapeutic drug hydroxyurea induced genetic and oxidative damage in an animal model. Environ Toxicol Pharmacol 60:91–99

Ahmed F, Husain Q (2019) Suppression in advanced glycation adducts of human serum albumin by bio-enzymatically synthesized gold and silver nanoformulations: a potential tool to counteract hyperglycemic condition. Biochimie 162:66–76

Ahmed F, Qayyum S, Husain Q (2018) Benign nano-assemblages of silver induced by β galactosidase with augmented antimicrobial and industrial dye degeneration potential. Mater Sci Eng C 91:570–578

Ansari SA, Husain Q (2012) Potential applications of enzymes immobilized on/in nano materials: a review. Biotechnol Adv 30(3):512–523

Ansari SA, Husain Q, Qayyum S, Azam A (2011) Designing and surface modification of zinc oxide nanoparticles for biomedical applications. Food Chem Toxicol 49(9):2107–2115

Barwal I, Sood A, Sharma M, Singh B, Yadav SC (2013) Development of stevioside pluronic-F-68 copolymer based PLA-nanoparticles as an antidiabetic nanomedicine. Colloids Surf B Biointerfaces 101:510–516

Bathina S, Srinivas N, Das UN (2017) Streptozotocin produces oxidative stress, inflammation and decreases BDNF concentrations to induce apoptosis of RIN5F cells and type 2 diabetes mellitus in Wistar rats. Biochem Biophys Res Commun 486(2):406–413

Buege JA, Aust SD (1978) Microsomal lipid peroxidation. Methods Enzymol 52:302–310

Egefjord L, Petersen AB, Bak AM, Rungby J (2010) Zinc, alpha cells and glucagon secretion. Curr Diabetes Rev 6(1):52–57

Farooqui Z, Ahmed F, Rizwan S, Shahid F, Khan AA, Khan F (2017) Protective effect of *Nigella sativa* oil on cisplatin induced nephrotoxicity and oxidative damage in rat kidney. Biomed Pharmacother 85:7–15

Ferdinando G, Brownlee M (2010) Oxidative stress and diabetic complications. Circ Res 107(9):1058–1070

Freeland RA, Harper AE (1959) Metabolic adaptations in higher animals V: the study of metabolic pathways by means of metabolic adaptations. J Biol Chem 234:1350–1354

Gaillet S, Rouanet JM (2015) Silver nanoparticles: their potential toxic effects after oral exposure and underlying mechanisms—a review. Food Chem Toxicol 77:58–63

Gray P (1954) The Microtomist's formulary and guide. Blakiston, New York, pp 403–409

Haider T, Husain Q (2007) Preparation of lactose-free milk by using salt-fractionated almond (*Amygdalus communis*) β-galactosidase. J Sci Food Agric 87:1278–1283

Haider T, Husain Q (2009) Hydrolysis of milk/whey lactose by β galactosidase: a comparative study of stirred batch process and packed bed reactor prepared with calcium alginate entrapped enzyme. Chem Eng Process 48(1):576–580

Hartmut J, Ramachandran A (2011) Reactive oxygen species in the normal and acutely injured liver. J Hepatol 55(1):227–228

He X, Li J, Wang B, Yao Q, Li L, Song R, Shi X, Zhang JA (2017) Diabetes self-management education reduces risk of all-cause mortality in type 2 diabetes patients: a systematic review and meta-analysis. Endocrine 55(3):712–731

Husain Q (2010) β Galactosidases and their potential applications: a review. Crit Rev Biotechnol 30(1):41–62

Husain Q (2018) Nanocarriers immobilized proteases and their industrial applications: an overview. J Nanosci Nanotechnol 18(1):486–499

Husain Q, Ansari SA, Alam F, Azam A (2011) Immobilization of *Aspergillus oryzae* β galactosidase on zinc oxide nanoparticles via simple adsorption mechanism. Int J Biol Macromol 49(1):37–43

Jansen J, Karges W, Rinkm L (2009) Zinc and diabetes-clinical links and molecular mechanisms. J Nutr Biochem 20(6):399–417

Jialal I, Sokoll LJ (2015) Clinical utility of lactate dehydrogenase: a historical perspective. Am J Clin Path 143(2):158–159

Jollow DJ, Mitchell JR, Zampaglione N, Gillette JR (1974) Bromobenzene induced liver necrosis: protective role of glutathione and evidence for 3,4-bromobenzene oxide as the hepatotoxic metabolite. Pharmacology 11:151–169

Jones AAD, Mi G, Webster TJ (2018) A status report on FDA approval of medical devices containing nanostructured materials. Trends Biotechnol 37(2):117–120

Kamaly N, Xiao Z, Valencia PM, Radovic-Moreno AF, Farokhzad OC (2012) Targeted polymeric therapeutic nanoparticles: design, development and clinical translation. Chem Soc Rev 41(7):2971–3010

Kind PRN, King EJ (1954) Estimation of plasma phosphatase by determination of hydrolysed phenol with amino-antipyrine. J Clin Pathol 7:322

Kornberg A (1955) Lactic dehydrogenase of muscle. Methods Enzymol 1:441–443

Levine RL, Williams JA, Stadtman EP, Shacter E (1994) Carbonyl assays for determination of oxidatively modified proteins. Methods Enzymol 233:346–357

Marklund S, Marklund G (1974) Involvement of the superoxide anion radical in the autoxidation of pyrogallol and a convenient assay for superoxide dismutase. FEBS J 47:469–474

Meyer JA, Spence DM (2009) A perspective on the role of metals in diabetes: past findings and possible future directions. Metallomics 1:32–41

Nagajyothi PC, Cha SJ, Yang IJ, Sreekanth TV, Kim KJ, Shin HM (2015) Antioxidant and anti-inflammatory activities of zinc oxide nanoparticles synthesized using *Polygala tenuifolia* root extract. J Photochem Photobiol B Biol 146:10–17

Nancy L, Keating A, O'Malley J, Smith MR (2006) Diabetes and cardiovascular disease during androgen deprivation therapy for prostate cancer. J Clin Oncol 24(27):4448–4456

Nickerson HD, Dutta S (2012) Diabetic complications: current challenges and opportunities. J Cardiovasc Transl Res 5(4):375–379

Niedowicz DM, Daleke DL (2005) The role of oxidative stress in diabetic complications. Cell Biochem Biophys 43(2):289–330

Reitman S, Frankel S (1957) A colorimetric method for the determination of serum glutamic oxalacetic and glutamic pyruvic transaminases. Am J Clin Pathol 28:56–63

Sedlak J, Lindsay RH (1968) Estimation of total protein bound and non-protein bound SH groups in tissue with Ellman's reagent. Ann Biochem 2:192–205

Seo K, Choi M, Jung UJ, Kim H, Yeo J, Jeon S, Lee M (2008) Effect of curcumin supplementation on blood glucose, plasma insulin, and glucose homeostasis related enzyme activities in diabetic db/db mice. Mol Nutr Food Res 52:995–1004

Sharma V, Anderson D, Dhawan A (2012) Zinc oxide nanoparticles induce oxidative DNA damage and ROS-triggered mitochondria mediated apoptosis in human liver cells (HepG2). Apoptosis 17(8):852–870

Shonk CC, Boxer GE (1964) Enzyme patterns in human tissues I: methods for the determination of glycolytic enzymes. Cancer Res 24:709–721

Shull KH, Ashmore J, Mayer J (1956) Hexokinase, glucose-6-phosphatase and phosphorylase levels in hereditary obese hyperglycemic mice. Arch Biochem Biophys 62:210–216

Tahrani AA, Bailey CJ, Prato SD, Barnett AH (2011) Management of type 2 diabetes: new and future developments in treatment. Lancet 378(9786):182–197

Trinder P (1969) Determination of glucose in blood using glucose oxidase with an alternative oxygen acceptor. Ann Clin Biochem 6:24–27

Valavanidisa A, Vlahogiannia T, Dassenakisb M, Scoullosb M (2006) Molecular biomarkers of oxidative stress in aquatic organisms in relation to toxic environmental pollutants. Ecotoxicol Environ Saf 64:178–189

Valgimigli L, Baschieria A, Amorati R (2018) Antioxidant activity of nanomaterials. J Mater Chem B 6:2036–2051

Ventola CL (2017) Progress in nanomedicine: approved and investigational nanodrugs. P&T Peer Rev J Formul Manag 42(12):742–755

Volpe CMO, Villar-Delfino PH, Dos Anjos PMF, Nogueira-Machado JA (2018) Cellular death, reactive oxygen species (ROS) and diabetic complications. Cell Death Dis 9(2):119

Zhang ZY, Xiong HM (2015) Photoluminescent ZnO nanoparticles and their biological applications. Materials 8(6):3101–3127

Zhang J, Qin X, Wang B, Xu G, Qin Z, Wang J, Wu L, Ju X, Bose DD, Qiu F, Zhou H, Zou Z (2017) Zinc oxide nanoparticles harness autophagy to induce cell death in lung epithelial cells. Cell Death Dis 8(7):e2954

**Publisher's Note** Springer Nature remains neutral with regard to jurisdictional claims in published maps and institutional affiliations.